fined quantitatively, then a more elaborate artificial vasomotor center can be developed that automatically adjusts the parameters. Automated adjustments may also be accomplished with adaptive control systems that execute real-time system identification and self-tuning of controller. The present study suggests the necessity of such manipulation of the vasomotor center settings.

Pressor and depressor responses by ESCS. We demonstrated both depressor and pressor responses in AP to ESCS with a linear range (Fig. 2). Earlier studies have shown that dorsal column stimulation produces pressor and depressor responses. Depressor response is produced by a group of dorsal column fibers that project to the dorsal nuclei at the level of C_8 to L_1 and transmit to the fibers that ascend through the dorsal spinocerebeller tracts (4, 27, 32). Pressor response is produced by another group of fibers that ascends or descends through the terminal zone and enter the gray matter. Some of these fibers project to the intermedial lateral columns to activate sympathetic presynaptic fibers. AP responses to ESCS observed in the present study are the results of compound responses in these multiple pathways. Nevertheless, controllability of AP by the BBS is ascertained by a clear linearity between ESCS and AP response in both static and dynamic relationships.

Although we have not confirmed it in the closed-loop condition, depressor response shown in the open-loop condition indicates that ESCS-mediated BBS can attenuate hypertension as well as hypotension. Because an offset ESCS rate (s_o) is applied in the absence of pressure disturbance, lowering ESCS rate would attenuate hypertension to some extent. AP in conscious animals fluctuates between hypertension and hypotension, even in a quiet position (5). The speed of AP restoration is considered sufficient to control these fluctuations.

Future step for clinical application. Clearly, the next step toward clinical application is to demonstrate the safety and the effectiveness of the ESCS-mediated BBS during orthostasis in conscious patients and animals. To study BBS in conscious animals, we have been developing an implantable hardware that enables BBS. Elaboration of such devices is mandatory for its future clinical application by searching the optimal stimulating site and condition that do not cause uncomfortable sensation and muscle twitch. A control algorithm must be developed that overcomes the problem revealed in the present study. The developing implant would be as small and low power as a pacemaker, with the aid of recent LSI technologies, and would be telemetrically programmable. In parallel, we began collaboration with a clinical group to develop ESCS-mediated BBS to suppress sudden hypotension in anesthetized humans during surgery. This study would prove the feasibility of human BBS.

Finally, new methods for long-term manometry are definitely required. Intravascular manometry can be achieved only with long-lasting antithrombotic material. Other indirect methods should be used until we are confident in antithrombotic ability.

Conclusions. As a step toward clinical application of BBS, we demonstrated that AP could be controlled with ESCS. We designed the artificial vasomotor center based on the dynamic characteristics of AP response to ESCS. Although there was a dissociation between the predicted and actual attenuation of AP fall, ESCS-mediated BBS with appropriate gain adjustment was capable of preventing HUT-induced hypotension rapidly, sufficiently, and stably.

APPENDIX

Simulation of AP Restoration and Implementation by the Artificial Vasomotor Center

We modeled the vasomotor center transfer function (G_c) as

$$G_c(f) = K_c \frac{1 + \frac{f}{f_{c1}}j}{\left(1 + \frac{f}{f_{c2}}j\right)\left(1 + \frac{f}{f_{c3}}j\right)} \exp(-2\pi f j L_c) \qquad (A1)$$

where f is frequency, K_c is the steady-state gain of the artificial vasomotor center, f_{c1} is f_c for derivative characteristics, f_{c2} and f_{c3} are corner frequencies for high-cut characteristics, j is an imaginary unit, and L_c is a pure delay. The value f_{c2} was set to $10 \times f_{c1}$, and f_{c3} was set to 1 Hz. These settings attenuate AP pulsation and preserve total baroreflex gain (13). L_c was introduced to simulate the possible time delay of 0.1 s in transforming AP to ESCS rate but was excluded in real-time application to improve AP stability.

The simulation was performed as follows. The block diagram in Fig. 4*A* is represented as

$$AP = G_p \cdot ESCS + P_d$$

$$ESCS = G_c \cdot AP$$

where G_p is transfer function of the peripheral effectors, and P_d is pressure disturbance to AP. Rearranging these formula yields

$$AP = G_c \cdot G_p \cdot AP + P_d \qquad (A2)$$

The time domain representation of *Eq. A2* is

$$\Delta AP(t) = \int g(\tau) \cdot \Delta AP(t - \tau)d\tau + P_d(t) \qquad (A3)$$

where $\Delta AP(t)$ is AP change from control value, and $g(\tau)$ is the impulse response function of the total open-loop transfer function ($G_c \cdot G_p$). To simulate orthostatic hypotension, $P_d(t)$ is set as an exponential AP fall to -60 mmHg with a time constant of 5 s rather than a stepwise fall (see Fig. 6*A*, *top*). We simulated the transient AP response to depressor stimulus while changing f_{c1} in the presence of the negative feedback system.

To implement the designed vasomotor center transfer function, we programmed the artificial vasomotor center to calculate ESCS rate in response to AP changes, according to the following equation:

$$ESCS(t) = \int h(\tau) \cdot \Delta AP(t - \tau)d\tau + s_o$$

where $h(\tau)$ is the impulse response function of the designed vasomotor center transfer function, $\Delta AP(t)$ is AP change from the control value, and s_o is the offset ESCS rate obtained from the static parameterization.

GRANTS

This study was supported by a Grant-in-Aid for Scientific Research (A15200040) from the Japan Society for the Promotion of Science, the Program for Promotion of Fundamental Studies in Health Science of Pharmaceuticals and Medical Devices Agency of Japan, and a Health and Labour Sciences Research Grant (Research on Advanced Medical Technology, H14-nano-002) from the Ministry of Health, Labour and Welfare of Japan.

REFERENCES

1. **Bannister R, da Costa DF, Hendry WG, Jacobs J, and Mathias CJ.** Atrial demand pacing to protect against vagal overactivity in sympathetic autonomic neuropathy. *Brain* 109: 345–356, 1986.

2. **Biaggioni I, Robertson RM, and Robertson D.** Manipulation of norepinephrine metabolism with yohimbine in the treatment of autonomic failure. *J Clin Pharmacol* 34: 418–423, 1994.
3. **Chobanian AV, Volicer L, Tifft CP, Gavras H, Liang CS, and Faxon D.** Mineralocorticoid-induced hypertension in patients with orthostatic hypotension. *N Engl J Med* 301: 68–73, 1994.
4. **Chung JM and Wurster RD.** Ascending pressor and depressor pathways in the cat spinal cord. *Am J Physiol* 231: 786–792, 1976.
5. **Cowley AW Jr, Liard JF, and Guyton AC.** Role of baroreceptor reflex in daily control of arterial blood pressure and other variables in dogs. *Circ Res* 32: 564–576, 1973.
6. **Di Pede F, Lanza GA, Zuin G, Alfieri O, Rapati M, Romano M, Circo A, Cardano P, Bellocci F, Santini M, and Maseri A; Investigators of the Prospective Italian Registry of SCS for Angina Pectoris.** Immediate and long-term clinical outcome after spinal cord stimulation for refractory stable angina pectoris. *Am J Cardiol* 91: 951–955, 2003.
7. **Frankel HL and Mathias CJ.** Severe hypertension in patients with high spinal cord lesions undergoing electro-ejaculation–management with prostaglandin E2. *Paraplegia* 18: 293–299, 1980.
8. **Glantz SA.** *Primer of Biostatistics* (4th ed.). New York: McGraw-Hill, 1997.
9. **Guyton AC, Coleman TG, and Granger HJ.** Circulation: overall regulation. *Annu Rev Physiol* 34: 13–46, 1972.
10. **Ikeda Y, Kawada T, Sugimachi M, Kawaguchi O, Shishido T, Sato T, Miyano H, Matsuura W, Alexander J Jr, and Sunagawa K.** Neural arc of baroreflex optimizes dynamic pressure regulation in achieving both stability and quickness. *Am J Physiol Heart Circ Physiol* 271: H882–H890, 1996.
11. **Illert M and Gabriel M.** Descending pathways in the cervical cord of cats affecting blood pressure and sympathetic activity. *Pflügers Arch* 335: 109–124, 1972.
12. **Kachi T, Iwase S, Mano T, Saito M, Kunimoto M, and Sobue I.** Effect of L-threo-3,4-dihydroxyphenylserine on muscle sympathetic nerve activities in Shy-Drager syndrome. *Neurology* 38: 1091–1094, 1988.
13. **Kawada T, Zheng C, Yanagiya Y, Uemura K, Miyamoto T, Inagaki M, Shishido T, Sugimachi M, and Sunagawa K.** High-cut characteristics of the baroreflex neural arc preserve baroreflex gain against pulsatile pressure. *Am J Physiol Heart Circ Physiol* 282: H1149–H1156, 2002.
14. **Kristinsson A.** Programmed atrial pacing for orthostatic hypotension. *Acta Med Scand* 214: 79–83, 1983.
15. **Malliani A, Pagani M, Lombardi F, and Cerutti S.** Cardiovascular neural regulation explored in the frequency domain. *Circulation* 84: 482–492, 1991.
16. **Marmarelis PZ and Marmarelis VZ.** *Analysis of Physiological Systems: The White-Noise Approach.* New York: Plenum, 1978.
17. **Matthews JM, Wheeler GD, Burnham RS, Malone LA, and Steadward RD.** The effects of surface anaesthesia on the autonomic dysreflexia response during functional electrical stimulation. *Spinal Cord* 35: 647–651, 1997.
18. **Meglio M, Cioni B, Rossi GF, Sandric S, and Santarelli P.** Spinal cord stimulation affects the central mechanisms of regulation of heart rate. *Appl Neurophysiol* 49: 139–146, 1986.
19. **Mehlsen J and Boesen F.** Substantial effect of acute hydration on blood pressure in patients with autonomic failure. *Clin Physiol* 7: 243–246, 1987.
20. **Obara A, Yamashita H, Onodera S, Yahara O, Honda H, and Hasebe N.** Effect of xamoterol in Shy-Drager syndrome. *Circulation* 85: 606–611, 1992.
21. **Parikh SM, Diedrich A, Biaggioni I, and Robertson D.** The nature of the autonomic dysfunction in multiple system atrophy. *J Neurol Sci* 200: 1–10, 2002.
22. **Robertson D.** Diagnosis and management of baroreflex failure. *Primary Cardiol* 21: 37–40, 1995.
23. **Sato T, Kawada T, Inagaki M, Shishido T, Takaki H, Sugimachi M, and Sunagawa K.** New analytic framework for understanding sympathetic baroreflex control of arterial pressure. *Am J Physiol Heart Circ Physiol* 276: H2251–H2261, 1999.
24. **Sato T, Kawada T, Shishido T, Sugimachi M, Alexander J Jr, and Sunagawa K.** Novel therapeutic strategy against central baroreflex failure: a bionic baroreflex system. *Circulation* 100: 299–304, 1999.
25. **Sato T, Kawada T, Inagaki M, Shishido T, Sugimachi M, and Sunagawa K.** Dynamics of sympathetic baroreflex control of arterial pressure in rats. *Am J Physiol Regul Integr Comp Physiol* 285: R262–R270, 2003.
26. **Sato T, Kawada T, Sugimachi M, and Sunagawa K.** Bionic technology revitalizes native baroreflex function in rats with baroreflex failure. *Circulation* 106: 730–734, 2002.
27. **Schramm LP and Livingston RH.** Inhibition of renal nerve sympathetic activity by spinal stimulation in rat. *Am J Physiol Regul Integr Comp Physiol* 252: R514–R525, 1987.
28. **Shannon JR, Diedrich A, Biaggioni I, Tank J, Robertson RM, Robertson D, and Jordan J.** Water drinking as a treatment for orthostatic syndromes. *Am J Med* 112: 355–360, 2002.
29. **Shimoji K, Hokari T, Kano T, Tomita M, Kimura R, Watanabe S, Endoh H, Fukuda S, Fujiwara N, and Aida S.** Management of intractable pain with percutaneous epidural spinal cord stimulation: differences in pain-relieving effects among diseases and sites of pain. *Anesth Analg* 77: 110–116, 1993.
30. **Shy M and Drager GA.** A neurological syndrome associated with orthostatic hypotension: a clinico-pathologic study. *Arch Neurol* 2: 511–527, 1960.
31. **Sugimachi M, Imaizumi T, Sunagawa K, Hirooka Y, Todaka K, Takeshita A, and Nakamura M.** A new method to identify dynamic transduction properties of aortic baroreceptors. *Am J Physiol Heart Circ Physiol* 258: H887–H895, 1990.
32. **Taylor RF and Schramm LP.** Spinally mediated inhibition of abdominal and lumbar sympathetic activities. *Am J Physiol Regul Integr Comp Physiol* 254: R655–R658, 1988.
33. **Wilcox CS, Puritz R, Lightman SL, Bannister R, and Aminoff MJ.** Plasma volume regulation in patients with progressive autonomic failure during changes in salt intake or posture. *J Lab Clin Med* 104: 331–339, 1984.

Effect of Electrical Modification of Cardiomyocytes on Transcriptional Activity through 5′-AMP-activated Protein Kinase

Yoshihiko Kakinuma, Yanan Zhang†, Motonori Ando*, Tetsuro Sugiura†, and Takayuki Sato**

Abstract: Endothelin-1 (ET-1) is known as an aggravating factor of the failing cardiomyocytes and, therefore, a therapeutic method is indispensable to decrease cardiac ET-1 expression. To study the mechanisms of how cardiac ET-1 gene expression can be modified, we investigated the effect of electrical stimulation against cardiomyocytes. Considering the physiology of cardiomyocytes, in vitro cultured cardiomyocytes demonstrate distinctive features from in vivo cardiomyocytes (i.e. the absence of a stretch along with electrical stimulation). In this study, we especially focused on the effect of electrical stimulation. The electrical stimulation reduced the gene expression of ET-1 mRNA in rat primary cultured cardiomyocytes. Furthermore, this effect on the transcriptional modification of ET-1 was also identified in H9c2 cells. Luciferase activity using H9c2 cells was decreased by electrical stimulation in the early phase, suggesting that the attenuation of the ET-1 gene transcription by electrical stimulation should be due to a transcriptional repression. To further investigate a trigger signal involved in the transcriptional repression, phosphorylation of 5′-AMP-activated protein kinase (AMPK) was evaluated. It was revealed that AMPK was phosphorylated in the early phase of electrical stimulation of H9c2 cells as well as in rat primary cultured cardiomyocytes, and that AMPK phosphorylation was followed by ET-1 transcriptional repression, suggesting that electrical stimulation directly regulates AMPK. This study suggests that AMPK activation in cardiomyocytes plays a crucial role in the transcriptional repression of ET-1.

Key Words: endothelin-1, cardiomyocytes, 5′-AMP-activated protein kinase

(*J Cardiovasc Pharmacol*™ 2004;44(suppl 1):S435–S438)

The endothelin (ET) system is known to be indispensable for the development of the heart. In the developmental stage, ET-1 exerts the formation of the heart through the receptors endothelin-A and endothelin-B, and the system exerts the biological function through either autocrine or paracrine fashion. It has been reported that deformity of the heart is produced in the absence of the ET system. Especially, cardiomyocytes have been reported to remarkably express and produce ET-1 in the pathophysiological condition (i.e. the failing heart) compared with the normal heart.[1] The mechanisms have been extensively studied of how the failing heart expresses ET-1 in the progression of heart failure; however, our previous study clearly demonstrated one aspect of the mechanisms — impaired cardiac energy metabolism.[2] The level of cardiac ET-1 gene expression is dependent on the condition of the cardiomyocytes in vivo; the failing cardiomyocytes produce more ET-1. However, even normal primary cultured cardiomyocytes in vitro could extraordinarily express ET-1 compared with in vivo. The abnormal pattern of cardiac ET-1 gene expression in vitro is also accompanied with a surprising switch of the myosin heavy chain isoform from α to β (a fetal pattern), suggesting that our cultured cardiomyocytes have already biologically changed their character.[3] However, this finding might provide us with some therapeutic clue as to how cardiac ET-1 expression can be depressed using cultured cardiomyocytes. If we could obtain some tool to repress cardiac ET-1 gene expression in vitro, it might lead to clarification of one of the therapeutic strategies against heart failure. Consequently we have so far concentrated on searching for ways to decrease cardiac ET-1 gene expression. Among them, we have found several methods to modify the expression using not chemicals or drugs, but physical stimulation.[3] In this study, using electrical stimulation (ES) we have successfully inhibited the cardiac ET-1 gene expression, and investigated the mechanisms by which such stimulation causes a depression of the gene expression.

METHODS

Cell Culture of Rat Cardiomyocytes and H9c2 Cells

According to our previous studies,[1] cardiomyocytes were isolated from 2-day-old Wistar–Kyoto rats. 5-Aminoimidazole-4-carboxamide-1-β-D-ribofuranosyl 5-monophosphate (AICAR) was purchased from Sigma (St Louis, MO, U.S.A.), and H9c2 cells were transiently treated by AICAR.

*Department of Cardiovascular Control and †Department of Laboratory Medicine, Kochi Medical School, Nankoku, Kochi, Japan
Address correspondence and reprint requests to Yoshihiko Kakinuma, Department of Cardiovascular Control, Kochi Medical School, Kohasu, Nankoku-shi, Kochi-ken 783-8505, Japan. E-mail: kakinuma@med.kochi-u.ac.jp
This study was supported by a Health and Labor Sciences Research Grant (H14-NANO-002) for Advanced Medical Technology from the Ministry of Health, Labor, and Welfare of Japan.

Electrical Stimulation

We have developed a specific ES device, which is modified to simultaneously provide multi-channels of ES and also to efficiently regulate bidirectional current. Our protocol for ES was performed as follows: 10 V, 10 milliseconds of duration and 4 Hz of frequency.

RNA Isolation and Reverse Transcription-Polymerase Chain Reaction

As previously described, total RNA was isolated, and 1 μg total RNA was reverse-transcribed and used for a polymerase chain reaction (PCR) template. PCR primers were prepared for preproET-1, hypoxia-inducible factor (HIF)-1α, β-actin,[2,3] and glucose transporter 3.

Luciferase Assay

As previously reported, the 5′-regulatory region of preproET-1 gene was subcloned into a luciferase vector.[2] The reporter vector was transfected into H9c2 cells by a cationic reagent, Effecten (QIAGEN, Valencia, CA, U.S.A.), according to the manufacture's protocol. Forty-eight hours after transfection, cells were lysed for evaluation of luciferase activity.

Western Blot Analysis

Cells were harvested from dishes by scraping, were washed with phosphate-buffered saline, and cell lysates were mixed with sample buffer. The samples were fractionated by sodium dodecyl sulfate-polyacrylamide gel electrophoresis and transferred onto membranes (Millipore Corp., Bedford, MA, U.S.A.). After transfer into the membrane, they were soaked in blocking buffer. The membranes were incubated with a monoclonal phosphor-5′-AMP-activated protein kinase-α (Thr172) antibody (1:1000; Cell Signaling Technology, Beverly, MA, U.S.A.). After the membranes were washed, horseradish peroxidase-conjugated secondary antibodies (Promega, Madison, WI, U.S.A.) were applied and the signal was detected using an enhanced chemi-luminescence system (Amersham, Piscataway, NJ, U.S.A.).

RESULTS

Electrical Stimulation Affects Gene Expression of Rat Cardiomyocytes

To investigate transcriptional regulation of cardiomyocytes, primary cultured cardiomyocytes were subjected to ES. Even with a bi-directional current, cardiomyocytes could not be cultured for ES more than 16 hours. As demonstrated in Fig. 1, ES remarkably decreased gene expression of preproET-1 and HIF-1α in the cardiomyocytes, compared with non-stimulated cardiomyocytes. However, the mRNA level of β-actin was not decreased by ES. Adversely, gene expression of glucose transporter 3 mRNA was increased by ES. These results suggested that

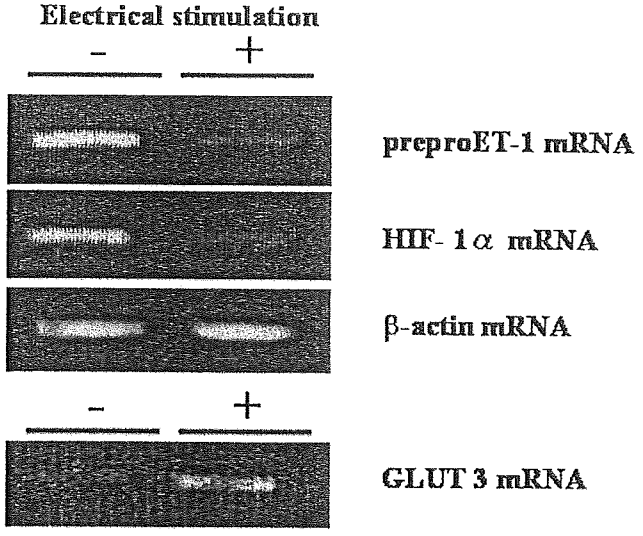

FIGURE 1. Electrical stimulation (ES) modifies gene expression of preproendothelin-1 (preproET-1), hypoxia-inducible factor-1α (HIF-1α), and glucose transporter (GLUT) 3 mRNAs. PreproET-1 and HIF-1α gene expressions were decreased 5 hours after ES. In contrast, GLUT 3 gene expression was increased by ES. The level of β-actin mRNA was not affected by ES.

cardiomyocytes respond to ES with an increased gene expression of glucose transporter 3; however, in contrast, such an ES modified gene expression of cardiac preproET-1 and HIF-1α.

Electrical Stimulation Transcriptionally Regulates PreproET-1 Gene Expression

Further to investigate especially the gene expression of preproET-1 mRNA, a reporter assay was performed using a reporter vector possessing the 5′-promoter regulatory region of the preproET-1 gene. H9c2 cells, a cell line of rat ventricular cardiomyocytes, were transfected by the reporter vector. As shown in Fig. 2, ES of H9c2 cells greatly decreased the luciferase activity of preproET-1. The phenomenon of the depressed luciferase activity was compatible with the decreased preproET-1 mRNA by reverse transcription-PCR.

Electrical Stimulation Elevates Phosphorylation of 5′-AMP-activated Protein Kinase

To investigate mechanisms to decrease a transcriptional level of preproET-1, we studied whether ES activates the phosphorylation of 5′-AMP-activated protein kinase (AMPK) using H9c2 cells. The time course study demonstrated that AMPK phosphorylation was detected soon after ES (Fig. 3). Furthermore, such an increase in AMPK phosphorylation was also observed in primary cultured cardiomyocytes. It was suggested that ES causes activation of

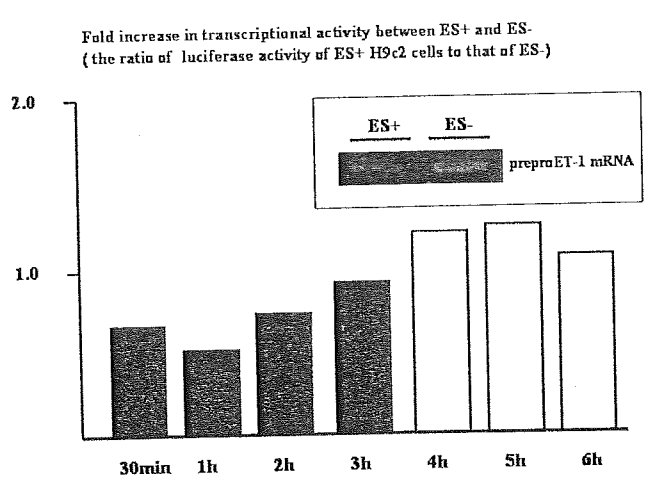

FIGURE 2. Electrical stimulation (ES) transcriptionally represses preproendothelin-1 (preproET-1) gene expression in H9c2 cells. Gene expression of preproET-1 in H9c2 cells was also decreased by ES. Using a reporter vector of the preproET-1 gene, luciferase activity was compared between electrical stimulated (ES+) H9c2 cells and non-electrical stimulated (ES–) cells. The ratio of luciferase activity of ES+ to that of ES– was measured, where a ratio > 1 suggests transcriptional activation, contrasting with a ratio < 1 suggesting repression.

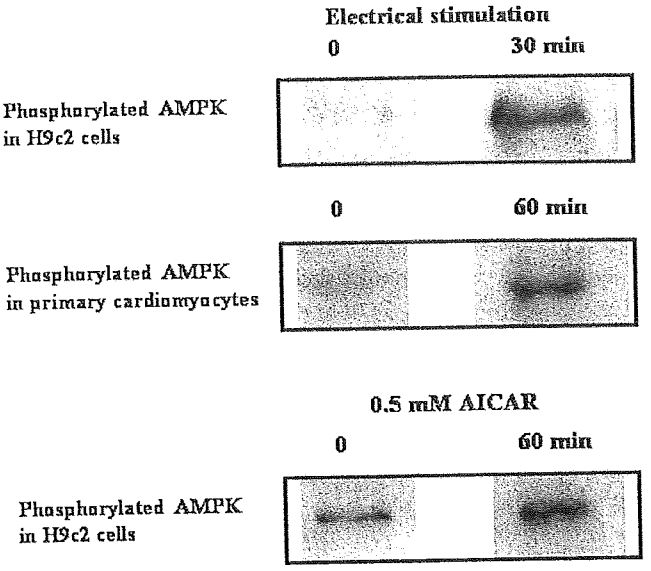

FIGURE 3. 5′-AMP-activated protein kinase (AMPK) is activated through phosphorylation by electrical stimulation (ES). ES caused activation of AMPK through phosphorylation in H9c2 cells. This phenomenon was also detected in rat primary cultured cardiomyocytes with a comparable time course. Also, 0.5 m*M* 5-aminoimidazole-4-carboxamide-1-β-D-ribofuranosyl 5-monophosphate (AICAR), an activator of AMPK, phosphorylated AMPK.

AMPK with a comparable time course of suppression of the preproET-1 gene, and consequently that AMPK phosphorylation is profoundly related to the repression of transcriptional activity of preproET-1 gene expression.

An Activator of AMPK Causes a Decrease in PreproET-1 mRNA

H9c2 cells were treated by AICAR, which is known as an activator of AMPK. As demonstrated in Fig. 3, AICAR increased the phosphorylation of AMPK. The activation of AMPK occurred very rapidly with a comparable time course of ES. With treatment of AICAR, the mRNA level of preproET-1 was decreased (Fig. 4). It was suggested that AMPK activation was involved in the attenuated preproET-1mRNA gene expression.

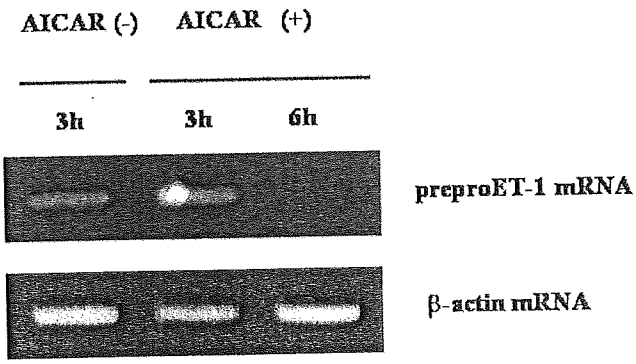

FIGURE 4. 5′-AMP-activated protein kinase activator decreases preproendothelin-1 (preproET-1) gene expression in H9c2 cells. 5-Aminoimidazole-4-carboxamide-1-β-D-ribofuranosyl 5-monophosphate (AICAR) 1.5 m*M* treatment remarkably decreased the gene expression of preproET-1 mRNA in H9c2 cells.

DISCUSSION

ET-1 is one of the aggravating factors in heart failure, because ET-1 further activates the glycolytic system in the failing cardiomyocytes, resulting in aggravation of malfunction in the heart. Therefore, one of the therapeutic goals that inhibit the progression of heart failure might be to decrease cardiac ET-1 gene expression. There are many manipulations to decrease ET-1 gene expression, including blocking the renin–angiotensin system and ET receptor antagonists.[4] However, we have further investigated whether other manipulations can modify the cardiac ET-1 expression, and then finally we have identified that a mechanical stimulation (i.e. ES) decreases cardiac ET-1 expression through activation of AMPK.

AMPK is known as a fuel sensor kinase, which is activated through phosphorylation when a cellular adenosine triphosphate (ATP) level is decreased.[5] Consequently, cells respond to a shortage of the energy and activate the

phosphorylation of AMPK. This kinase is therefore activated in the early phase to stimuli that might cause mitochondrial dysfunction, leading to ATP deprivation. This response through AMPK phosphorylation is considered an adaptation of cells to avoid cellular death with a shortage of ATP. However, this response is not only involved in pathological states, but also in physiological states. For example, exercise-induced muscle hypertrophy leads to remarkable adaptation of the muscle to the more efficient utilization of energy (i.e. mitochondrial β-oxidation of fatty acid), and consequently to activation of the mitochondrial function.[6] In the case of exercise, AMPK in skeletal muscle is known to be activated.[7] Therefore, it is suggested that the activation of AMPK through phosphorylation is followed by enhancement of mitochondrial function in a physiological condition to obtain more adequate ATP.

It is known that the cardiomyocytes obtain ATP predominantly through mitochondrial β-oxidation of fatty acid; however, when cardiomyocytes were treated by hypoxia, the cardiac energy metabolic system was changed from β-oxidation to glycolysis, because fatty acid oxidation is impaired. In such a case, as our previous study demonstrated, HIF-1α is induced for upregulation of glycolytic enzymes, and furthermore HIF-1α transcriptionally activates preproET-1 gene expression in the failing heart.[2] It is suggested that cardiac ET-1 expression is accompanied with a cellular glycolysis-dominant energy system.[8] With these findings in mind, further speculation is as follows: if the glycolysis-dominant energy system is inhibited, and alternatively mitochondrial β-oxidation of fatty acid is activated, ET-1 gene expression could be decreased. As our present study demonstrated, ES activates the phosphorylation of AMPK in a rapid fashion, followed by a decrease in the transcriptional activity of ET-1.

This is a first demonstration of transcriptional repression of cardiac preproET-1 gene expression using methods other than drugs. Moreover, this reaction is very rapid to decrease preproET-1 mRNA. Therefore, it is suggested that the manipulation of cardiomyocytes by ES is one candidate method to inhibit an increase in cardiac ET-1 gene expression.

REFERENCES

1. Kakinuma Y, Miyauchi T, Kobayashi T, et al. Myocardial expression of endothelin-2 is altered reciprocally to that of endothelin-1 during ischemia of cardiomyocytes *in vitro* and during heart failure *in vivo*. *Life Sci.* 1999;65:1671–1683.
2. Kakinuma Y, Miyauchi T, Yuki K, et al. Novel molecular mechanism of increased myocardial endothelin-1 expression in the failing heart involving the transcriptional factor hypoxia inducible factor-1α induced for impaired myocardial energy metabolism. *Circulation.* 2001;103: 2387–2394.
3. Kakinuma Y, Miyauchi T, Suzuki T, et al. Enhancement of glycolysis in cardiomyocytes elevates endothelin-1 expression through the transcriptional factor HIF-1α. *Clin Sci.* 2002;103(suppl. 48):210S–214S.
4. Sakai S, Miyauchi T, Kobayashi T, et al. Inhibition of myocardial endothelin pathway improves lomg-term survival in heart failure. *Nature.* 1996;384:353–355.
5. Winder WW. Energy-sensing and signaling by AMP-activated protein kinase in skeletal muscle. *J Appl Physiol.* 2001;91:1017–1028.
6. Saha AK, Schwarsin AJ, Roduit R, et al. Activation of malonyl-CoA decarboxylase in rat skeletal muscle by contraction and the AMP-activated protein kinase activator 5-aminoimidazole-4-carboxamide-1-β-D-ribofuranoside. *J Biol Chem.* 2000;275:24279–24283.
7. Hood DA. Plasticity in skeletal, cardiac, and smooth muscle invited review: contractile activity-induced mitochondrial biogenesis in skeletal muscle. *J Appl Physiol.* 2001;90:1137–1157.
8. Wu-Wong JR, Berg CE, Kramer D. Endothelin stimulates glucose uptake via activation of endothelin-A receptor in neonatal rat cardiomyocytes. *J Cardiovasc Pharmacol.* 2000;36(5 suppl. 1): S179–S183.

Innovative Methodology

Am J Physiol Heart Circ Physiol 287: H2906–H2913, 2004;
doi:10.1152/ajpheart.00035.2004.

A self-calibrating telemetry system for measurement of ventricular pressure-volume relations in conscious, freely moving rats

Kazunori Uemura,[1] Toru Kawada,[1] Masaru Sugimachi,[1] Can Zheng,[1,2,3] Koji Kashihara,[1,3] Takayuki Sato,[4] and Kenji Sunagawa[1]

[1]*Department of Cardiovascular Dynamics, National Cardiovascular Center Research Institute, Suita 565-8565;* [2]*Japan Space Forum, Tokyo 105-0013;* [3]*Organization of Pharmaceutical Safety and Research, Tokyo 100-0013; and* [4]*Department of Cardiovascular Control, Kochi Medical School, Nankoku 783-8505, Japan*

Submitted 15 January 2004; accepted in final form 28 July 2004

Uemura, Kazunori, Toru Kawada, Masaru Sugimachi, Can Zheng, Koji Kashihara, Takayuki Sato, and Kenji Sunagawa. A self-calibrating telemetry system for measurement of ventricular pressure-volume relations in conscious, freely moving rats. *Am J Physiol Heart Circ Physiol* 287: H2906–H2913, 2004; doi:10.1152/ajpheart.00035.2004.—Using Bluetooth wireless technology, we developed an implantable telemetry system for measurement of the left ventricular pressure-volume relation in conscious, freely moving rats. The telemetry system consisted of a pressure-conductance catheter (1.8-Fr) connected to a small (14-g) fully implantable signal transmitter. To make the system fully telemetric, calibrations such as blood resistivity and parallel conductance were also conducted telemetrically. To estimate blood resistivity, we used four electrodes arranged 0.2 mm apart on the pressure-conductance catheter. To estimate parallel conductance, we used a dual-frequency method. We examined the accuracy of calibrations, stroke volume (SV) measurements, and the reproducibility of the telemetry. The blood resistivity estimated telemetrically agreed with that measured using an ex vivo cuvette method ($y = 1.09x - 11.9$, $r^2 = 0.88$, $n = 10$). Parallel conductance estimated by the dual-frequency (2 and 20 kHz) method correlated well with that measured by a conventional saline injection method ($y = 1.59x - 1.77$, $r^2 = 0.87$, $n = 13$). The telemetric SV closely correlated with the flowmetric SV during inferior vena cava occlusions ($y = 0.96x + 7.5$, $r^2 = 0.96$, $n = 4$). In six conscious rats, differences between the repeated telemetries on different days (3 days apart on average) were reasonably small: 13% for end-diastolic volume, 20% for end-systolic volume, 28% for end-diastolic pressure, and 6% for end-systolic pressure. We conclude that the developed telemetry system enables us to estimate the pressure-volume relation with reasonable accuracy and reproducibility in conscious, untethered rats.

conductance catheter; serial reproducibility; volumetric accuracy; dual-frequency method; Bluetooth

SMALL EXPERIMENTAL ANIMALS, such as rats and mice, are widely used in cardiovascular research. These animals can offer a variety of disease models, including heart failure and hypertension, and enable us to analyze the molecular mechanisms of the pathophysiology underlying such diseases (5, 7, 12, 21, 27). To interpret the molecular findings in terms of cardiac phenotype, an accurate assessment of cardiac function, including the contractile properties of the left ventricle (LV), is required. As a load-insensitive index of LV contractility, the end-systolic pressure-volume relation (ESPVR) has been estimated in small animal species with the use of a conductance catheter technique or an ultrasonic crystal method in acute experimental settings (6, 9, 14, 15, 23). However, the anesthesia and thoracotomy required by these techniques inevitably exert adverse effects on the heart (13, 22, 30). In addition, the time course of disease progression or long-term drug effects cannot be assessed in acute experimental settings (7, 16). To overcome these problems, long-term experimental settings should be developed where the LV pressure-volume relation can be measured telemetrically in small experimental animals.

In the present study, we have developed a new telemetry system to measure LV volume, pressure, and electrocardiogram (ECG) in conscious, freely moving rats. In this system, the LV pressure-volume relation was obtained from a pressure-conductance catheter chronically implanted in the rat LV. To calibrate the conductance signal and obtain absolute LV volume, measurements of blood resistivity (ρ) and parallel conductance (G_p) are required (3, 4). These calibration procedures require blood sampling and hypertonic saline infusion, but such ex vivo procedures are not applicable to conscious, freely moving small animals. To circumvent such ex vivo procedures in our new telemetry system (29), we adopted a self-calibrating method for the LV volume measurement, as reported in our previous study (28). The aim of the present study was therefore to develop a telemetry system and evaluate its performance. Our results indicate that we succeeded in measuring the LV pressure-volume relation in conscious, untethered rats with reasonable accuracy and reproducibility.

METHODS

Implantable Pressure-Volume Telemetry System

Figure 1*A* illustrates a newly developed pressure-volume telemetry system for rats; it consists of a pressure-conductance catheter, an analog processor-transmitter (weight = 14 g, volume = 11 ml), and a battery unit (lithium battery; weight = 12 g, volume = 10 ml).

Pressure-conductance catheter. Details of the pressure-conductance catheter are presented in Fig. 1*B*. To measure LV conductance, four platinum electrodes (0.25 mm wide) were used. Constant excitation current was applied to the two outermost electrodes while the voltage signal associated with LV conductance was measured from the two inner sensing electrodes. To measure LV pressure, a high-fidelity pressure transducer (Millar Instruments, Houston, TX) was mounted between the two sensing electrodes for the LV conductance measurement. To measure ρ, four smaller platinum electrodes (0.1 mm wide, 0.2 mm between centers of adjacent electrodes, 0.6 mm

Address for reprint requests and other correspondence: K. Uemura, Dept. of Cardiovascular Dynamics, National Cardiovascular Center Research Institute, 5-7-1, Fujishirodai, Suita 565-8565, Japan (E-mail: kuemura@ri.ncvc.go.jp).

The costs of publication of this article were defrayed in part by the payment of page charges. The article must therefore be hereby marked "*advertisement*" in accordance with 18 U.S.C. Section 1734 solely to indicate this fact.

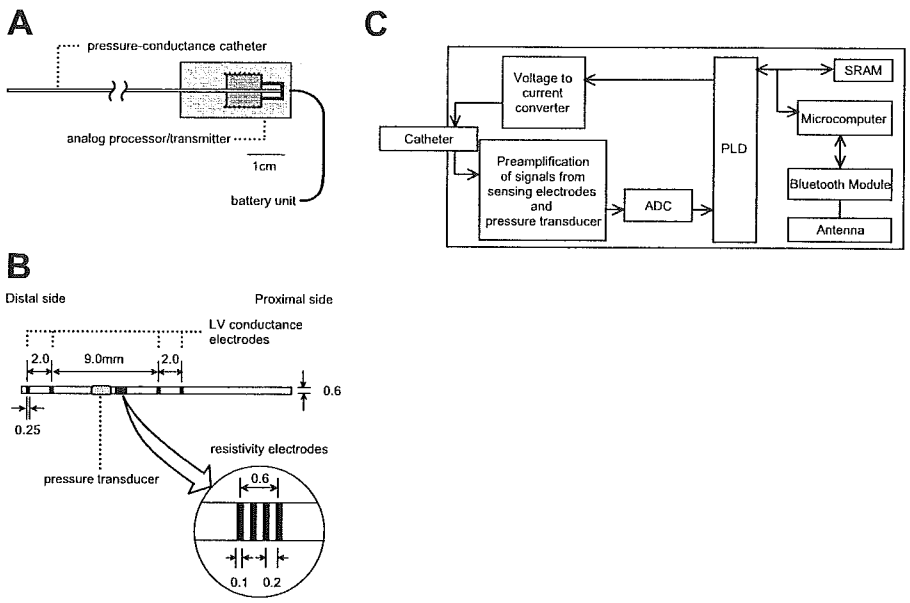

Fig. 1. *A*: schematic illustration of our pressure-volume telemetry system. A 10-cm-long pressure-conductance catheter obtains signals of left ventricular (LV) conductance and pressure, intraventricular blood resistivity, and an ECG. Signals are processed and transmitted by an analog processor transmitter, which is powered by a battery unit (lithium battery). *B*: schematic illustration of our pressure-conductance catheter. Catheter has 4 electrodes for measurement of LV conductance and 4 electrodes for measurement of intraventricular blood resistivity (*inset*). A high-fidelity pressure transducer is mounted between *electrodes 2* and *3*. *C*: block diagram of an analog processor transmitter. ADC, analog-to-digital converter; PLD, programmable logic device; SRAM, static random access memory.

between centers of excitation electrodes) were placed near the pressure transducer (Fig. 1*B*, *inset*). Constant excitation current was applied to the two outer electrodes while the voltage signal associated with ρ was measured from the two inner electrodes.

Analog processor transmitter. A block diagram of the analog processor transmitter is presented in Fig. 1*C*. It was equipped with several functions. First, it delivered a dual-frequency (2 and 20 kHz) constant excitation current [20 μA root mean square (RMS)] for measurements of LV conductance and ρ. We validated the current output by injecting it into known resistors and examining the developed voltage. The resulting RMS current output was 20.4 μA (SD 0.2) and 19.3 μA (SD 0.2) at 2 and 20 kHz, respectively. These values were constant over different resistors (50–990 Ω). Second, it measured and processed the voltage signal from the sensing electrodes as follows: Analog signals were digitized (12 bits, 40-kHz sampling rate; model ADS7870, Texas Instruments, Dallas, TX) and then fed into a programmable logic device (model XC 2C256, Xilinx, San Jose, CA), which processed them to yield RMS digital signals corresponding to frequency components of 2 and 20 kHz and a low-frequency signal (<2 kHz; see APPENDIX). The circuit was connected to the larger or smaller electrodes in response to a command signal, so that LV conductance or ρ could be measured. Third, the analog processor-transmitter had a bridge amplifier for the LV pressure measurement. The LV pressure signal was also digitized (12 bits, 40-kHz sampling rate). All these functions were controlled by a microcomputer (model H8S, Hitachi, Tokyo, Japan).

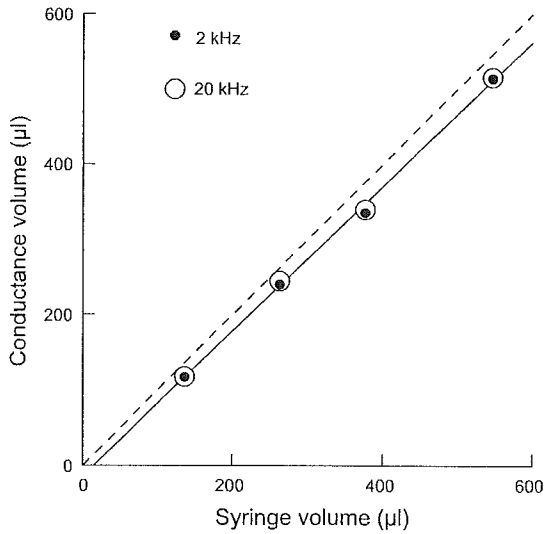

Fig. 2. Comparison of conductance-derived volumes at 2 and 20 kHz vs. known fluid volumes of syringes. Both conductance-derived volumes were essentially identical for each of the syringe volumes. Relation between conductance-derived volume and syringe volume was quite linear. Solid line, regression between conductance-derived volume at 20 kHz and syringe volume; dashed line, identity.

Bluetooth technology was used to transmit the data (18). For real-time monitoring, all processed signals were resampled at 200 Hz by the microcomputer and transmitted to an external receiver (CA-SIRA, CSR, Cambridge, UK) by a Bluetooth module (model LMBTB027, Murata, Tokyo, Japan). For high-precision non-real-time analysis, signals recorded at 2,000 Hz over a 6-s interval were stored in a static random access memory (model HM62V16256, Hitachi) and then transmitted to the receiver by the Bluetooth module. The external receiver detected the radio-frequency signal from the transmitter and converted it to a serial bit stream.

Self-Calibration of Ventricular Volumetry

The principles of conductance volumetry have been described previously (3, 4). Briefly, the ventricular conductance signal (G) can be converted to absolute ventricular volume (V) as follows

$$V = (1/\alpha)\,(L^2 \cdot \rho)\,(G - G_p) \qquad (1)$$

where α is a volume calibration factor, L is the distance between the sensing electrodes, ρ is blood resistivity, and G_p is parallel conductance. L was 9 mm in the present catheter design.

In a preliminary experiment, when the catheter was placed in a series of graduated syringes filled with diluted saline, conductance-derived volumes at 2 and 20 kHz were close to the true syringe volume in the volume range of interest (Fig. 2). Conductance-derived volumes at the two frequencies were essentially identical for each of the syringe volumes. Hence, α was assumed to be unity in the present study (14, 23).

The four smaller electrodes were used to estimate ρ (Fig. 1*B*, *inset*). The distance between the excitation electrodes was set at 0.6 mm. In an in vitro experiment, we confirmed that the current distribution volume was confined to an ~4-mm diameter around the catheter with this electrode design (see APPENDIX). The end-diastolic LV diameter is 7–9 mm in normal rats and 9–12 mm in rats with left heart failure (17). Because the interelectrode distance between the excitation electrodes was small enough to confine the current distribution volume to within the end-diastolic ventricular blood pool in the rat LV, we estimated ρ at end diastole (10, 28).

G_p was estimated by the dual-frequency excitation method (8, 9, 28) as follows

$$G_p = \kappa \times \Delta G_{20-2} \quad (2)$$

where ΔG_{20-2} is the difference in ventricular conductance values between the 20- and 2-kHz excitation frequencies and κ is an experimentally derived constant. Once κ is determined, G_p can be estimated from ΔG_{20-2}, obviating the need for saline infusion.

Instrumentation and Experimental Protocols

Thirty-three male Sprague-Dawley rats (350–400 g body wt) were used. Care of the animals was in strict accordance with the *Guiding Principles for the Care and Use of Animals in the Field of Physiological Sciences* as approved by the Physiological Society of Japan. The animals were anesthetized with pentobarbital sodium (50 mg/kg ip) and ventilated artificially. A vertical midline cervical incision was made to expose the right common carotid artery while the animal was in the supine position. The pressure-conductance catheter of the telemetry system was inserted into the LV retrogradely from the right common carotid artery. The position of the catheter was verified by monitoring the pressure-volume signal and by two-dimensional echocardiography. At the conclusion of the experiment, the animal was killed with an overdose of pentobarbital sodium, and the heart was examined to reconfirm the proper positioning of the catheter.

Group 1 (n = 23). We evaluated the accuracy of telemetric calibration of ρ and G_p under anesthetized, closed-chest conditions. Catheters (3-Fr) were inserted into the right and left jugular veins for blood sampling and saline injection, respectively. In 10 of the 23 rats, we compared ρ estimated telemetrically (ρ_{est}) with ρ measured from sampled blood by a conventional ex vivo cuvette method (ρ_{conv}). In the remaining 13 rats, we estimated G_p by the dual-frequency excitation method ($G_{p,est}$) and by the hypertonic saline method ($G_{p,conv}$). To obtain $G_{p,conv}$, we injected 20 μl of saturated saline into the right jugular vein while continuously measuring LV conductance (14, 23). To obtain $G_{p,est}$, we measured LV conductance at 2- and 20-kHz excitation frequencies and derived ΔG_{20-2} by averaging the instantaneous conductance difference over ~10 cardiac cycles. We randomly selected 7 of the 13 rats and determined the proportionality constant (κ in *Eq. 2*) from the averaged ratio of $G_{p,conv}$ to ΔG_{20-2}. $G_{p,est}$ and $G_{p,conv}$ were measured while the artificial ventilation was temporarily suspended at end expiration.

Group 2 (n = 4). Under anesthetized, open-chest conditions, we evaluated the accuracy of volumetry by comparing stroke volume (SV) measured by the telemetry system with SV measured by an ultrasonic flowmeter (model 2.5S273, Transonic Systems, Ithaca, NY). After median sternotomy, the aortic arch was dissected free from surrounding tissues. A flow probe was placed around the ascending aorta to measure the aortic blood flow. A string occluder was placed loosely around the inferior vena cava to decrease the LV preload and vary the SV over a wide range. We simultaneously measured the telemetric LV volume and the ultrasonic aortic blood flow while varying the preload. The measurements were done while the artificial ventilation was temporarily suspended at end expiration.

Group 3 (n = 6). Under conscious, closed-chest conditions, we evaluated the reproducibility of the telemetry on different days. Aseptic conditions were maintained throughout the surgical procedure. The telemetry system was implanted in a subcutaneous pocket made at the right upper dorsum. The skin was closed, and the animal was allowed to recover from anesthesia. On the day after implantation surgery, the LV volume, pressure, and an ECG were measured telemetrically in the fully recovered, conscious animal (*study 1*). Each rat underwent a second set of telemetric measurements at 1–6 days after the initial study (*study 2*). Ambient barometric pressure was measured simultaneously and subtracted from the telemetric LV pressure to compensate for changes in atmospheric pressure.

Data Collection

We used the real-time mode (200-Hz sampling) of the telemetry system and recorded LV conductance, LV pressure, intraventricular ECG, and ρ on a hard disk of a dedicated laboratory computer system (model HFPA031003, Epson, Tokyo, Japan). In *group 2*, ultrasonic aortic blood flow was digitized at 1,000 Hz through a 12-bit analog-to-digital converter and stored on a hard disk for subsequent analyses.

Statistical Analysis

For the calculation of LV volume using *Eq. 1*, *G* and ρ were obtained from the 20-kHz frequency component. In *group 1*, we used linear regression analysis to compare the telemetric and conventional measurements of ρ (ρ_{est} vs. ρ_{conv}) and G_p ($G_{p,est}$ vs. $G_{p,conv}$). In *group 2*, we calculated the telemetric SV from the difference between the end-diastolic volume (EDV) and end-systolic volume (ESV) in each beat. The flowmetric SV was computed from the time integral of aortic blood flow. The telemetric SV was compared with the flowmetric SV by linear regression analysis. In *group 3*, we compared heart rate (HR), EDV, ESV, end-diastolic pressure (EDP), and end-systolic pressure (ESP) between *study 1* and *study 2* for each rat. Using the pressure-volume data, we calculated ejection fraction (EF), maximal pressure increase ($+dP/dt_{max}$) or decrease ($-dP/dt_{max}$) over time, and the time constant of isovolumic relaxation (τ) and compared them between *study 1* and *study 2* for each rat. A nonparametric multiple comparison (Wilcoxon's signed-rank test) was used to examine the difference in each parameter between *study 1* and *study 2*. Group data are expressed as means (SD). Differences were considered significant at $P < 0.05$.

RESULTS

Telemetric Calibration of ρ

Figure 3*A* is a representative time series showing LV pressure and ρ at 2 and 20 kHz derived from the telemetry. The bottom of the ρ waveform, which corresponded to end diastole, represents the time when there was sufficient blood volume around the catheter (10). The lowest ρ values at 2 kHz ($\rho_{2\,kHz}$) and 20 kHz ($\rho_{20\,kHz}$) were very close (197 and 207 Ω·cm, respectively). This was the case for all the rats, indicating that ρ was frequency independent ($\rho_{2\,kHz} = 1.08\rho_{20\,kHz} - 13.8$, $r^2 = 0.96$, SE of the estimate = 6.7 Ω·cm) (6, 9). The lowest ρ at 20 kHz was treated as ρ_{est}.

Figure 3*B* summarizes the relation between ρ_{est} and ρ_{conv} obtained from 10 rats in *group 1*. ρ_{est} agreed with ρ_{conv} reasonably well ($\rho_{est} = 1.09\rho_{conv} - 11.9$, $r^2 = 0.88$, SE of the estimate = 10.7 Ω·cm). The ratio of SE of the estimate to the mean of ρ_{est} was 0.046, indicating small variability around the regression line.

Telemetric Calibration of G_p

Figure 4*A* illustrates a representative time series of telemetrically measured ECG, LV conductance signals at 2 and 20 kHz, and LV pressure. In this animal, ΔG_{20-2} was 0.56 mS

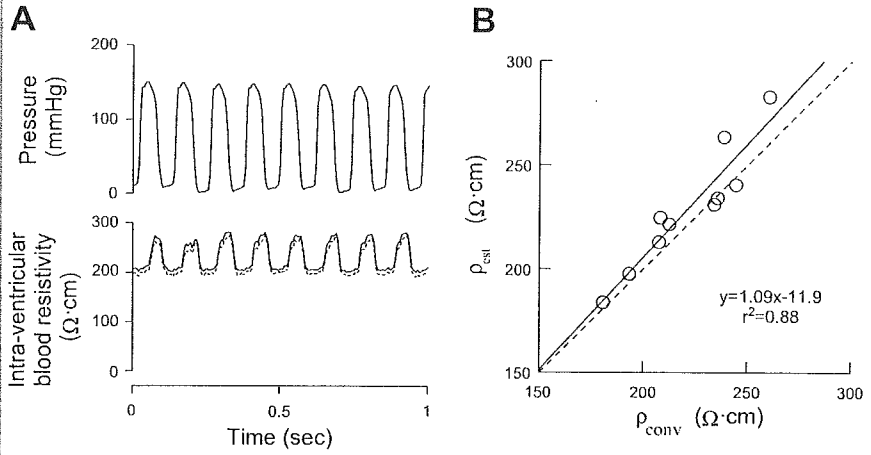

Fig. 3. *A*: waveforms of ventricular pressure and intraventricular blood resistivity at 2 kHz (dashed line) and 20 kHz (solid line) as a function of time obtained telemetrically. *B*: relation between blood resistivity as measured in a cuvette (ρ_{conv}) and as estimated via catheter electrodes (ρ_{est}) in 10 rats. Solid line, regression; dashed line, identity.

and $G_{p,conv}$ was 3.27 mS. Therefore, κ was calculated to be 5.79 from *Eq. 2* in this animal. The averaged κ from seven randomly selected rats was 5.14, which we used as the experimentally derived constant to obtain $G_{p,est}$ for all rats.

Figure 4*B* summarizes the relation between $G_{p,est}$ and $G_{p,conv}$ obtained from 13 rats in *group 1*. $G_{p,est}$ correlated well with $G_{p,conv}$ ($G_{p,est} = 1.59G_{p,conv} - 1.77$, $r^2 = 0.87$, SE of the estimate = 0.33 mS). The ratio of SE of the estimate to the mean of $G_{p,est}$ was 0.11, indicating that the estimation was reasonable around the mean of $G_{p,est}$.

Accuracy of the Televolumetry

Figure 5*A* depicts LV pressure and volume measured by telemetry and aortic blood flow measured by the ultrasonic flowmeter. Vena caval occlusion decreased LV pressure, volume, and aortic blood flow.

Figure 5*B* summarizes the relation between telemetric SV (SV_{tele}) and flowmetric SV (SV_{flow}) obtained from four rats in *group 2*. SV_{tele} matched SV_{flow} reasonably well in each of the four rats: $r^2 = 0.90$–0.99, slope = 0.86 (SD 0.16), intercept = 12.4 μl (SD 10.4), and SE of the estimate = 4.3 μl (SD 0.4). A linear regression analysis on the pooled data from all four rats also showed a highly linear relation between SV_{tele} and SV_{flow}: $SV_{tele} = 0.96SV_{flow} + 7.5$, $r^2 = 0.96$, SE of the estimate = 6.6 μl. The ratio of SE of the estimate to the mean of SV_{tele} was 0.10.

Reproducibility of the Telemetry

Individual data obtained by the telemetry system for all six rats in *group 3* are provided in Tables 1 and 2. The overall variability between repeated measurements in the same rat was reasonably small. There were no significant differences in repeated measurements of HR, EDV, ESV, EDP, and ESP between *study 1* and *study 2* (Table 1). There were no significant differences in repeated measurements of EF, $+dP/dt_{max}$, $-dP/dt_{max}$, and τ between *study 1* and *study 2* (Table 2).

Figure 6 illustrates the representative LV pressure-volume loops obtained from a rat in *group 3*. The pressure-volume loops in *studies 1* and *2* were almost identical.

DISCUSSION

We have developed a novel telemetry system for measurements of LV volume, pressure, and ECG in conscious, freely moving rats. The system, for the first time to the best of our knowledge, has enabled measurement of the LV pressure-

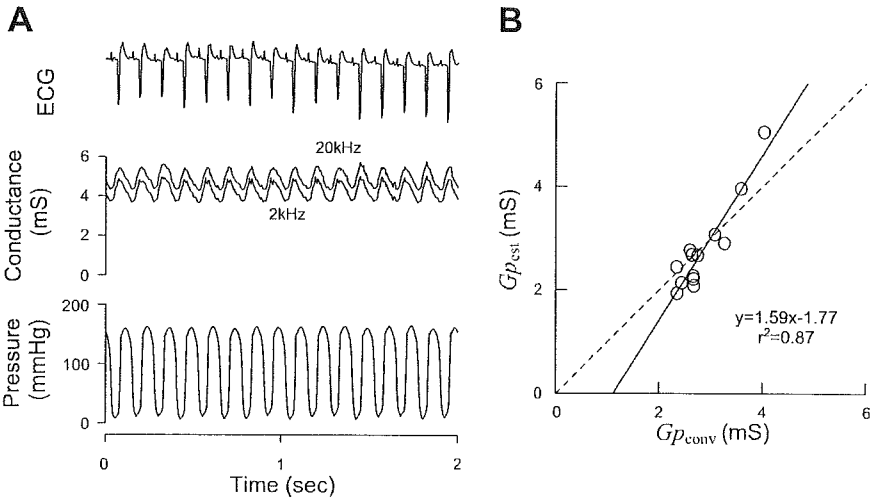

Fig. 4. *A*: waveforms of an ECG, conductance signals at 2 and 20 kHz, and ventricular pressure as a function of time, obtained telemetrically. *B*: relation between parallel conductance estimated by the saline infusion method ($G_{p,conv}$) and by dual-frequency excitation method ($G_{p,est}$) in 13 rats. Solid line, regression; dashed line, identity.

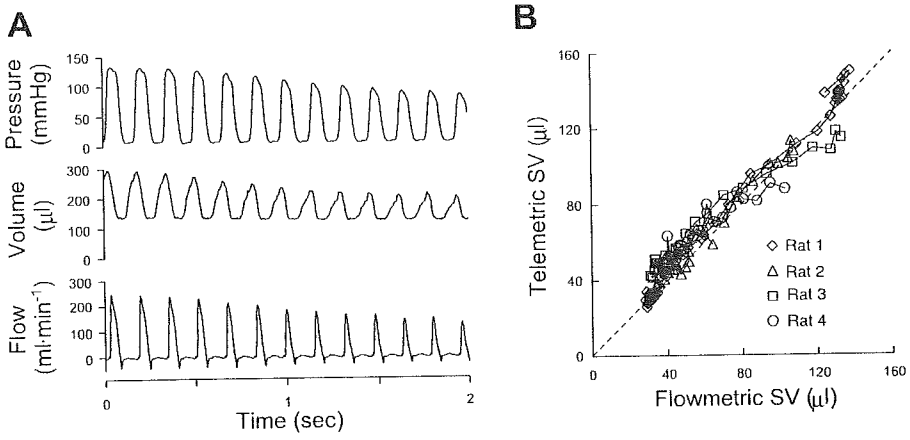

Fig. 5. *A*: representative traces of ventricular pressure, ventricular volume obtained telemetrically, and aortic flow measured by an ultrasonic flowmeter during vena cava occlusion in 1 rat. *B*: relation between telemetric stroke volume (SV) and flowmetric SV in 4 rats. Dashed line, identity.

volume relation in small experimental animals, such as rats, under completely conscious, unrestricted conditions with reasonably good accuracy and reproducibility.

Self-Calibrating Volumetry

In our conductance volumetric system, ρ and G_p were estimated using the telemetric signals alone (Figs. 3 and 4). We will be able to use the empirical constant κ (=5.14), determined in this study, in the future application of our telemetry system to rats. The self-calibrating feature made it possible to measure the LV pressure-volume relation in rats without tethering them for ex vivo calibration procedures, such as blood sampling and hypertonic saline infusion. Besides their impracticality in conscious, small animals, these procedures can alter hemodynamic conditions (6, 9). Frequent blood sampling can induce anemia. Concentrated saline injection depresses myocardial contractility and has volume-loading effects (6, 9). Our telemetry system is free of these problems.

The current used for resistivity measurements was distributed in a 2-mm radius around the catheter (see APPENDIX). The ratio of the radius (i.e., penetration depth) to the distance between the excitation electrodes was ~3 (≒2/0.6). This ratio is at odds with previously reported values, which were around or less than unity (6, 10, 26). Penetration depth is affected by the relation between the resistivity of the target tissue and that of the surrounding structure (26). This relation in our study was different from those in previous studies, which would be one reason for the discrepancy. Difference in shape and arrangement of the electrodes between our system and those previous studies would be another reason. Because the electrodes were placed very closely, stray capacitance between connecting wires could be a problem (31). The fact that resistivity values at 2 and 20 kHz were very close indicated that our titration method effectively removed the problem of stray capacitance (see APPENDIX). However, it might be better to incorporate techniques such as capacitance neutralization to completely prevent the problem, in case the capacitance were to significantly affect our titration accuracy in future long-term use, e.g., with increases in electrode impedance (31).

We used the dual-frequency excitation method previously described by Gawne et al. (8). Feldman et al. (6) combined measured resistivity of the myocardium with an analytic approach and estimated G_p from the conductance signals at 10 and 100 kHz. Although their method was completely independent of saline injection, it required measurement of myocardial resistivity with an additional four-electrode sensor.

Volumetric Accuracy and Reproducibility

We have verified the volumetric accuracy of our telemetry system by comparing SV_{tele} with SV_{flow} during inferior vena cava occlusions (Fig. 5*A*). The volumetric accuracy of the conductance catheter technique in the rat heart has been ex-

Table 1. *Reproducibility of hemodynamic variables*

	HR, beats/min		EDV, μl		ESV, μl		EDP, mmHg		ESP, mmHg	
Rat	S1	S2	S1	S2	S1	S2	S1	S2	S1	S2
1	530	475	303	307	168	182	14	19	131	123
2	363	476	310	280	212	151	11	17	121	133
3	426	500	330	355	212	220	12	9	127	129
4	405	511	244	194	143	89	14	13	120	125
5	402	382	364	434	269	326	15	14	119	106
6	400	380	240	283	158	167	24	36	142	152
Mean (SD)	421 (57.3)	454 (58.2)	299 (49)	309 (81)	194 (47)	189 (80)	15 (5)	18 (10)	127 (9)	128 (15)
Difference Mean (SD)	65 (40)		37 (23)		34 (26)		5 (4)		8 (4)	
Percent difference Mean (SD)	15 (9)		13 (8)		20 (17)		28 (16)		6 (4)	

S1, *study 1;* S2, *study 2;* HR, heart rate; EDV, left ventricular end-diastolic volume; ESV, left ventricular end-systolic volume; EDP, left ventricular end-diastolic pressure; ESP, left ventricular end-systolic pressure.

Table 2. *Reproducibility of parameters of ventricular functions*

Rat	EF, %		+dP/dt$_{max}$, mmHg/s		−dP/dt$_{max}$, mmHg/s		τ, ms	
	S1	S2	S1	S2	S1	S2	S1	S2
1	45	41	10,594	9,615	7,165	6,648	9.2	9.0
2	32	46	9,284	11,802	6,364	7,372	8.5	8.3
3	36	38	10,373	12,129	7,277	6,937	9.4	8.1
4	42	54	9,274	11,801	7,527	7,013	6.4	9.5
5	26	25	8,862	7,610	6,132	4,878	7.4	7.9
6	34	41	9,808	9,756	7,518	7,273	11.0	12.4
Mean (SD)	36 (7)	41 (10)	9,699 (682)	10,452 (1,773)	6,997 (601)	6,687 (923)	8.7 (1.6)	9.2 (1.7)
Difference								
Mean (SD)	7 (5)		1513 (957)		646 (397)		1.1 (1.1)	
Percent difference								
Mean (SD)	17 (13)		15 (9)		10 (7)		13 (14)	

EF, left ventricular ejection fraction; dP/dt$_{max}$, maximal pressure rise (+) or decrease (−) over time; τ, time constant of isovolumic left ventricular relaxation.

amined using a similar comparison (14, 23). Ito et al. (14) reported a very high and linear correlation (r = 0.97–0.99) between conductance-derived SV and SV measured by an electromagnetic flowmeter in rats. We also obtained a similar highly linear relation between SV_{tele} and SV_{flow} (Fig. 5*B*).

The reproducibility of our telemetry system (Table 1) is good enough for many applications, such as the study of LV remodeling in rats. This is because EDV has been reported to increase to ~200% of the control value in rats with ischemic heart failure and in heart failure-prone rats (2, 7, 12).

Applications of the Telemetry System

The developed telemetry system enables detailed evaluation of cardiac function in small animals by eliminating the effects of anesthesia and acute surgical intervention (13, 22, 30). By using a single-beat estimation method to determine the ESPVR, our system would enable evaluation of the load-independent contractile index in conscious animals (24, 25). We validated pressure-volume signals only under control conditions in this study. The stability of the acquired data and the capacity of our system to monitor altered hemodynamics remain to be evaluated.

Our telemetry system is potentially useful for the long-term monitoring of LV function. We confirmed that our system was viable for up to 8 days in this study. However, further studies are required to definitively evaluate the longevity of the implants over a longer period of time (19). Thrombosis and infection would affect the morbidity and mortality associated with the chronic implantation of our system. Coating of the pressure-conductance catheter with anticoagulants and further miniaturization of the implant are under development to ameliorate such problems.

We adopted Bluetooth technology for telecommunication. Bluetooth is a wireless technology designed to allow low-cost, short-range radio links between mobile personal computers and other portable devices (18). While point-to-point connections are supported, Bluetooth technology allows up to seven simultaneous connections to be established and maintained by a single receiver (18). This unique feature of Bluetooth technology should be beneficial in experimental settings where a large population of animals in a single cage must be evaluated (16).

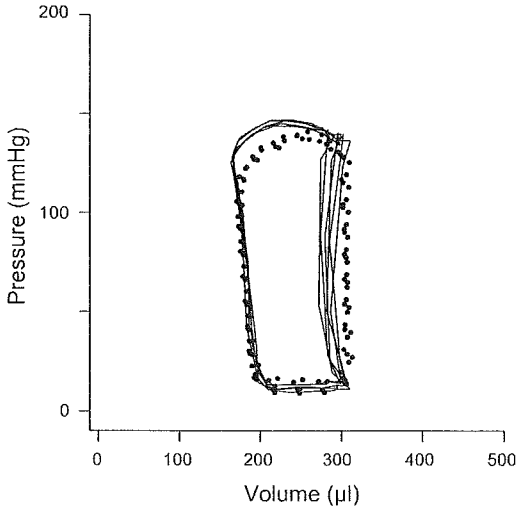

Fig. 6. Day-to-day reproducibility of LV pressure-volume loops in 1 rat. Thick solid loops, *study 1*; dotted loops, *study 2*. Loops for *studies 1* and *2* (6 days apart) were superimposable.

Limitations

The volume calibration factor α was assumed to be unity on the basis of the preliminary experiment, where the conductance-derived volume was close to true syringe volume in the normal operating range for rats (Fig. 2). Georgakopoulos and Kass (9) noted that the relation was quite linear when the volume range was limited to the physiological operating range for mice. Hettrick et al. (11) also noted that conductance-derived volume was close to true syringe volume and α was unity in a volume range. However, both groups and others noted that the relation was nonlinear when considered over a wider volume range (1, 9, 11, 20). In addition, the syringes have no G_p, whereas the rat heart does. It has been shown that G_p has significant effects on α (11). Taken together, these findings suggest that it will be necessary to recalibrate α when we apply our system to the rat LV in heart failure or other cardiac disorders, where drastic changes in ventricular volume and changes in the electrical properties of surrounding structures, i.e., change in G_p, are probable (1).

Values of EF in Table 2 are low for normal rats (5, 7). Other parameters of LV function are, however, within the normal

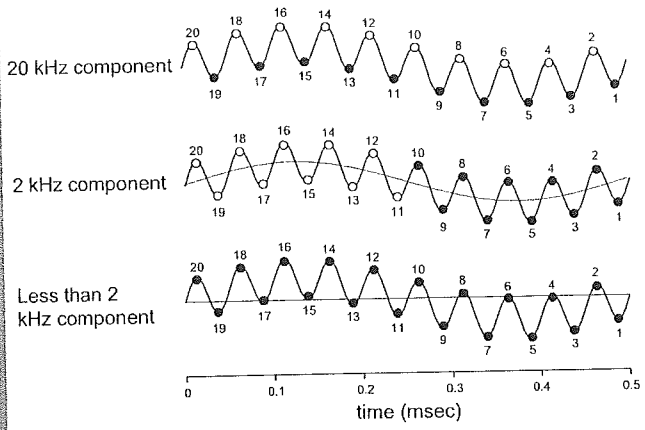

Fig. 7. Visual representation of logical processing used to extract 20-, 2-, and <2-kHz frequency components of digital signals.

range (5, 7) (Table 2). Dual-frequency derived G_p values from the rats in *group 3* ranged from 1.8 to 3.3 mS (mean 2.3 ± 0.4 mS). The dual-frequency method slightly underestimated G_p in that range compared with the saline injection method (Fig. 4*B*). This might result in an apparent reduction of EF. To settle the discrepancy between EF and other functional parameters, it is necessary to compare the telemetric EF with the EF determined by other independent methods, such as echocardiography.

We were able to estimate ρ in the LV cavity in normal-sized rats with the present catheter design (Fig. 1*B, inset*). However, the catheter design may not be applicable to smaller rats or mice, where the current distribution volume probably distributes outside the LV cavity. To apply our system to these small animals, further reduction of the interelectrode distance is required for measurement of ρ.

Conclusion

A novel telemetry system was developed for measurements of LV pressure, volume, and ECG in conscious, freely moving rats. The system enabled us to accurately measure the LV pressure-volume relation with good reproducibility and without the harmful effects of anesthesia or acute surgical trauma in rats.

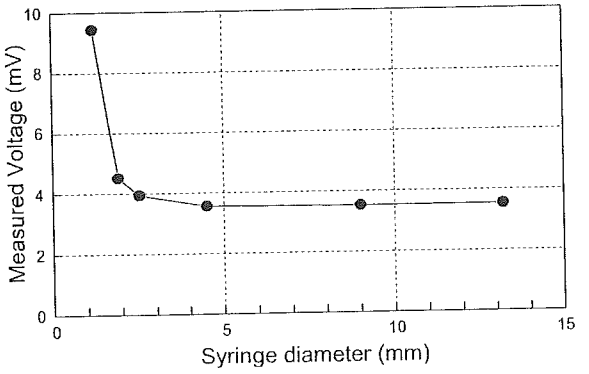

Fig. 8. Relation between syringe diameter and voltage as measured by sensing electrodes of our conductance catheter designed for blood resistivity measurement. Voltage reaches a minimum at a syringe diameter of ~4 mm. This indicates that current distribution volume is confined to within a 4-mm diameter around the catheter.

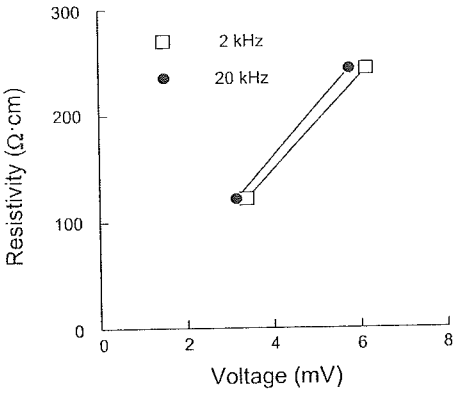

Fig. 9. Relation between measured voltage and saline resistivity.

APPENDIX

Logical processing of digital signals to extract frequency components. We extracted frequency components of 20 kHz, 2 kHz, and low frequency (<2 kHz) by logical processing of digital signals. The analog signals were converted to digital signals at a sampling rate of 40 kHz. Twenty serial digital values were processed simultaneously (Fig. 7). We obtained the 20-kHz component on the basis of the difference between even- and odd-numbered digital values. We calculated an average of every 10 digital values. We obtained the 2-kHz component on the basis of the difference between the two averaged values of the former half and the latter half (average of 10 values each). We obtained the low-frequency component by averaging all 20 digital values. All this logical processing was performed by the programmable logic device (Fig. 1*C*).

Estimation of intraventricular ρ. First, we experimentally determined the current distribution volume of the four small electrodes for estimation of ρ. We placed our pressure-conductance catheter at the center of plastic syringes of various sizes filled with diluted saline. Saline resistivity was matched to that of the blood (122 Ω·cm). We injected a constant current (20 kHz, 20 μA RMS) into the excitation electrodes (0.6 mm apart; Fig. 1*B, inset*) and measured voltage via the sensing electrodes. We present the relation between the measured voltage and the syringe diameter in Fig. 8. As demonstrated, with increasing syringe diameter, the voltage signal decreased and reached a minimum at a syringe diameter of ~4 mm. This implied that most (>95%) of the current was confined to within the cylindrical diameter at which the voltage reached a minimum. From these data, we concluded that the current distribution volume was confined to within a 4-mm diameter around the catheter.

Second, the resultant voltage signal was converted to ρ by a conversion formula. We determined the conversion formula experimentally by placing the catheter at the center of a plastic syringe with a diameter of 9 mm. Syringes were filled with diluted saline solutions with known resistivities in the range of those expected in rat blood (122 and 244 Ω·cm). Constant currents (20 and 2 kHz, 20 μA RMS) were injected between the excitation electrodes. We linearly related the measured RMS voltage to saline resistivity and used this relation as a conversion formula (Fig. 9).

ACKNOWLEDGMENTS

This study was presented in part at the Scientific Sessions of the American Heart Association, Orlando, FL, November 2003.

GRANTS

This study was supported by Ministry of Health Labour and Welfare of Japan Health and Labour Sciences Research Grants for Research on Advanced Medical Technology 13090401 and H14-Nano-002 and Japan Society for the Promotion of Science Grants-in-Aid for Scientific Research A 15200040, C

14570707, and C 15590786, by a Ground-Based Research Grant for space utilization promoted by the National Space Development Agency of Japan and the Japan Space Forum, and by the Program for Promotion of Fundamental Studies in Health Science of the Organization for Pharmaceutical Safety and Research of Japan.

REFERENCES

1. **Applegate RJ, Cheng CP, and Little WC.** Simultaneous conductance catheter and dimension assessment of left ventricle volume in the intact animal. *Circulation* 81: 638–648, 1990.
2. **Asanoi H, Ishizaka S, Kameyama T, Nozawa T, Miyagi K, and Sasayama S.** Serial reproducibility of conductance catheter volumetry of left ventricle in conscious dogs. *Am J Physiol Heart Circ Physiol* 262: H911–H915, 1992.
3. **Baan J, Jong TT, Kerkhof PL, Moene RJ, van Dijk AD, van der Velde ET, and Koops J.** Continuous stroke volume and cardiac output from intra-ventricular dimensions obtained with impedance catheter. *Cardiovasc Res* 15: 328–334, 1981.
4. **Baan J, van der Velde ET, de Bruin HG, Smeenk GJ, Koops J, van Dijk AD, Temmerman D, Senden J, and Buis B.** Continuous measurement of left ventricular volume in animals and humans by conductance catheter. *Circulation* 70: 812–823, 1984.
5. **Cingolani OH, Yang XP, Cavasin MA, and Carretero OA.** Increased systolic performance with diastolic dysfunction in adult spontaneously hypertensive rats. *Hypertension* 41: 249–254, 2003.
6. **Feldman MD, Mao Y, Valvano JW, Pearce JA, and Freeman GL.** Development of a multifrequency conductance catheter-based system to determine LV function in mice. *Am J Physiol Heart Circ Physiol* 279: H1411–H1420, 2000.
7. **Francis J, Weiss RM, Wei SG, Johnson AK, and Felder RB.** Progression of heart failure after myocardial infarction in the rat. *Am J Physiol Regul Integr Comp Physiol* 281: R1734–R1745, 2001.
8. **Gawne TJ, Gray KS, and Goldstein RE.** Estimating left ventricular offset volume using dual-frequency conductance catheters. *J Appl Physiol* 63: 872–876, 1987.
9. **Georgakopoulos D and Kass DA.** Estimation of parallel conductance by dual-frequency conductance catheter in mice. *Am J Physiol Heart Circ Physiol* 279: H443–H450, 2000.
10. **Gopakumaran B, Osborn P, Petre JH, and Murray PA.** A new technique to measure and track blood resistivity in intracardiac impedance volumetry. *J Clin Monit* 13: 363–371, 1997.
11. **Hettrick DA, Battocletti JH, Ackmann JJ, Linehan JH, and Warltier DC.** Effects of physical parameters on the cylindrical model for volume measurement by conductance. *Ann Biomed Eng* 25: 126–134, 1997.
12. **Heyen JR, Blasi ER, Nikula K, Rocha R, Daust HA, Frierdich G, Van Vleet JF, De Ciechi P, McMahon EG, and Rudolph AE.** Structural, functional, and molecular characterization of the SHHF model of heart failure. *Am J Physiol Heart Circ Physiol* 283: H1775–H1784, 2002.
13. **Hoit BD, Ball N, and Walsh RA.** Invasive hemodynamics and force-frequency relationships in open- versus closed-chest mice. *Am J Physiol Heart Circ Physiol* 273: H2528–H2533, 1997.
14. **Ito H, Takaki M, Yamaguchi H, Tachibana H, and Suga H.** Left ventricular volumetric conductance catheter for rats. *Am J Physiol Heart Circ Physiol* 270: H1509–H1514, 1996.
15. **Kubota T, Mahler CM, McTiernan CF, Wu CC, Feldman MD, and Feldman AM.** End-systolic pressure-dimension relationship of in situ mouse left ventricle. *J Mol Cell Cardiol* 30: 357–363, 1998.
16. **Lapointe N, Blais C Jr, Adam A, Parker T, Sirois MG, Gosselin H, Clement R, and Rouleau JL.** Comparison of the effects of an angiotensin-converting enzyme inhibitor and a vasopeptidase inhibitor after myocardial infarction in the rat. *J Am Coll Cardiol* 39: 1692–1698, 2002.
17. **Litwin SE, Katz SE, Morgan JP, and Douglas PS.** Serial echocardiographic assessment of left ventricular geometry and function after large myocardial infarction in the rat. *Circulation* 89: 345–354, 1994.
18. **Lou E, Fedorak MV, Hill DL, Raso JV, Moreau MJ, and Mahood JK.** Bluetooth wireless database for scoliosis clinics. *Med Biol Eng Comput* 41: 346–349, 2003.
19. **Mills PA, Huetteman DA, Brockway BP, Zwiers LM, Gelsema AJ, Schwartz RS, and Kramer K.** A new method for measurement of blood pressure, heart rate, and activity in the mouse by radiotelemetry. *J Appl Physiol* 88: 1537–1544, 2000.
20. **Mur G and Baan J.** Computation of the input impedances of a catheter for cardiac volumetry. *IEEE Trans Biomed Eng* 31: 448–453, 1984.
21. **Murphy AM, Kogler H, Georgakopoulos D, McDonough JL, Kass DA, Van Eyk JE, and Marban E.** Transgenic mouse model of stunned myocardium. *Science* 287: 488–491, 2000.
22. **Price HL and Ohnishi ST.** Effects of anesthetics on the heart. *Fed Proc* 39: 1575–1579, 1980.
23. **Sato T, Shishido T, Kawada T, Miyano H, Miyashita H, Inagaki M, Sugimachi M, and Sunagawa K.** ESPVR of in situ rat left ventricle shows contractility-dependent curvilinearity. *Am J Physiol Heart Circ Physiol* 274: H1429–H1434, 1998.
24. **Sato T, Shishido T, Miyashita H, Yoshimura R, and Sunagawa K.** Single-beat estimation of end-systolic elastance (E_{es}) in rats (Abstract). *Circulation* 96 *Suppl* I: I-518, 1997.
25. **Shishido T, Hayashi K, Shigemi K, Sato T, Sugimachi M, and Sunagawa K.** Single-beat estimation of end-systolic elastance using bilinearly approximated time-varying elastance curve. *Circulation* 102: 1983–1989, 2000.
26. **Steendijk P, Mur G, Van Der Velde ET, and Baan J.** The four-electrode resistivity technique in anisotropic media: theoretical analysis and application on myocardial tissue in vivo. *IEEE Trans Biomed Eng* 40: 1138–1148, 1993.
27. **Uechi M, Asai K, Osaka M, Smith A, Sato N, Wagner TE, Ishikawa Y, Hayakawa H, Vatner DE, Shannon RP, Homcy CJ, and Vatner SF.** Depressed heart rate variability and arterial baroreflex in conscious transgenic mice with overexpression of cardiac $G_s\alpha$. *Circ Res* 82: 416–423, 1998.
28. **Uemura K, Sugimachi M, Shishido T, Kawada T, Inagaki M, Zheng C, Sato T, and Sunagawa K.** Convenient automated conductance volumetric system. *Jpn J Physiol* 52: 497–503, 2002.
29. **Uemura K, Sugimachi M, and Sunagawa K.** Self-calibratable ventricular pressure-volume telemetry system for rats (Abstract). *Circulation* 108 *Suppl* IV: IV-37, 2003.
30. **Vatner SF and Braunwald E.** Cardiovascular control mechanisms in the conscious state. *N Engl J Med* 293: 970–976, 1975.
31. **Wood JW.** Stray-capacitance neutralisation for high-resistance microelectrodes—a simple analysis. *Med Biol Eng Comput* 19: 230–236, 1981.

高血圧治療における塩酸ベニジピンとＡⅡ受容体拮抗薬併用療法の検討

高知大学医学部
佐藤恭子[1]・山崎文靖[2]
古野貴志[1]・佐藤隆幸[3]
杉浦哲朗[2]・土居義典[1]

要　旨

本態性高血圧患者に対する塩酸ベニジピンとＡⅡ受容体拮抗薬併用療法の有用性と安全性を検討した。両剤の併用により良好な降圧効果が得られた。また，降圧による反射性頻脈や検査データの重篤な悪化，投薬を中止するような自覚症状の出現などの副作用も見られず，両剤の併用は高血圧治療において有用かつ安全であると考えられた。さらに，塩酸ベニジピンとＡⅡ受容体拮抗薬の投与順序による薬効差は認めず，また，併用するＡⅡ受容体拮抗薬の種類による降圧の程度および試験期間中を通じての脈拍にも差はなかった。以上より，塩酸ベニジピンとＡⅡ受容体拮抗薬との併用療法は単剤で効果不十分な症例において有用性が高く，安全性にも優れていると考えられた。

Combination Treatment with Benidipine Hydrochloride and Angiotensin II Receptor Blocker for Hypertension

Kyoko Sato[1], Fumiyasu Yamasaki[2], Takashi Furuno[1],
Takayuki Sato[3], Tetsuro Sugiura[2], Yoshinori Doi[1]
Kochi Medical School
1 : *Department of Medicine and Geriatrics*
2 : *Department of Clinical Laboratory*
3 : *Department of Cardiovascular Control*

1：老年病科・循環器科　2：検査部　3：循環制御学
連絡先：高知大学医学部老年病科・循環器科　〒783-8505　高知県南国市岡豊町小蓮
Tel：088-880-2352　Fax：088-880-2349　e-mail address:satok@med.kochi-u.ac.jp

I はじめに

これまで我が国では高血圧患者の治療において，降圧効果が確実であり，禁忌とされる疾患が少ないことから長時間作用型のCa拮抗薬が多く使用されてきた。しかし近年，合併症を伴う高血圧患者を対象とした心・脳血管事故発症に対する研究で，ACE阻害薬がCa拮抗薬より優れているという結果が報告[1)2)]され，またACE阻害薬と降圧効果や臓器保護効果が同等で，咳などの副作用が少なく安全性に優れたAII受容体拮抗薬が第一選択薬として使用される頻度が増加している[3)~6)]。

近年の大規模臨床試験において，十分な降圧が心血管イベントだけでなく脳血管障害のリスクを低下させることが明らかにされ[7)8)]，いくつかの高血圧診断治療指針でも1剤での降圧効果が不十分な場合，降圧の効率を高め，かつ副作用を軽減することができることより，少量多剤併用療法が推奨されている[9)~13)]。Ca拮抗薬は降圧効果が強力であることから，今後は単剤による治療だけでなくACE阻害薬やAII受容体拮抗薬と併用される機会が多くなることが予測される。実際，我が国ではCa拮抗薬やACE阻害薬が汎用されており[3)~6)]，その併用療法の有用性は多く報告[14)~18)]されている。

一方，Ca拮抗薬とAII受容体拮抗薬の併用時の有効性，および安全性についての検討はあまり見られない。そこで今回，ジヒドロピリジン系長時間作用型Ca拮抗薬である塩酸ベニジピンとAII受容体拮抗薬併用における高血圧治療の有用性と安全性を検討した。

II 方　　法

1. 対象と方法

収縮期血圧140mmHg以上，拡張期血圧90mmHg以上のどちらか一方を満たす外来通院中の本態性高血圧症患者に2週以上の観察期間を設け，その後，各薬剤の承認された通常投与量，すなわち塩酸ベニジピン4mg/日またはAII受容体拮抗薬（ロサルタン；50mg/日，カンデサルタン；8mg/日，バルサルタン；80mg/日，テルミサルタン；40mg/日）のいずれか一方を4週以上投与した。この時期を1剤投与期とし，血圧，脈拍，体重の測定，血液生化学検査および自覚症状の調査を実施した。1剤投与期の血圧が収縮期血圧140mmHg以上または拡張期血圧90mmHg以上であった患者に，先行投与薬剤の用法・用量を変えず，もう一方のクラスの薬剤を追加投与してこの時期を2剤併用期とした。併用開始後2週以上が経過した時点で1剤投与期と同様に血圧，脈拍，体重の測定，血液生化学検査および自覚症状の調査を実施した。観察期間にすでに投与されていた降圧薬は用法・用量を変更せずに継続した。継続した降圧薬の内訳はCa拮抗薬3例，ACE阻害薬1例，β遮断薬1例，利尿薬1例，α遮断薬1例であった。

重症高血圧（拡張期血圧120mmHg以上）患者，重症心不全患者，過去6カ月以内に発生した急性冠症候群および脳血管疾患患者，HbA_{1c}が7%以上の糖尿病患者は除外した。

2. 検討項目

血圧は座位にて医師または看護師が上腕動脈よりコロトコフ法にて測定し，同時に脈拍数，体重を測定した。

血液学的検査として，赤血球数，ヘモグロビン，ヘマトクリット，白血球数，血小板数を，生化学検査として，総蛋白，アルブミン，血糖，AST，ALT，総ビリルビン，CPK，総コレステロール，中性脂肪，BUN，クレアチニン，尿酸，Na，K，Cl，CRPを測定した。

可能な症例において胸部正面エックス線像を撮影，心胸郭比を計測し，心拡大の指標とした。

自覚症状は，観察期間に認められた症状の推移および試験期間中に新たに出現した症状を患者本人から聞き取った。

3. 副作用

試験期間中に新たに発現し，主治医が投薬を中止する必要があると判定した自・他覚症状を

表1 患　者　背　景

		全　例	AII受容体拮抗薬先行群	塩酸ベニジピン先行群	
n		38	27	11	
年齢（歳）		67±12	65±12	72±11	n.s.
性別（男性）		19	15	4	n.s.
収縮期血圧（mmHg）		168±21	167±19	170±26	n.s.
拡張期血圧（mmHg）		89±12	89±11	91±15	n.s.
脈拍数（/分）		74±10	75±10	73±10	n.s.
1剤投与期間（週）		36.1±36.1	31.3±30.0	39.1±49.7	n.s.
2剤併用期間（週）		36.3±44.4	35.1±34.6	39.1±64.6	n.s.
AII受容体拮抗薬の種類（例数）	・ロサルタン	21	14	7	
	・カンデサルタン	9	7	2	
	・バルサルタン	7	6	1	
	・テルミサルタン	1	0	1	

副作用として扱った。副作用の有無は受診毎に確認した。

また，臨床検査値は，1）正常値から異常値へ明らかに変化したとき，2）観察期間から異常値であったが試験期間中に明らかに増悪したとき，のそれぞれにおいて投与した薬剤との関連性が明確に否定された場合を除いて副作用として扱った。

4. 統計手法

結果は平均値±標準偏差で表した。有意差検定は反復測定ANOVAを用い，post hoc testはScheffeの方法を用いて検討した。有意水準は5％未満とした。

III 結　　果

全例，AII受容体拮抗薬先行群および塩酸ベニジピン先行群の背景を表1に示す。AII受容体拮抗薬先行群は27例で，その内訳は，ロサルタン14例，カンデサルタン7例，バルサルタン6例であった。塩酸ベニジピン先行群は11例で，2剤併用期のAII受容体拮抗薬の内訳は，ロサルタン7例，カンデサルタン2例，バルサルタン1例，テルミサルタン1例であった。投与前の年齢，性別，血圧値，脈拍，および1剤投与期間，2剤併用期間はAII受容体拮抗薬先行群と塩酸ベニジピン先行群の間に有意な差は認めなかった。

1. 血圧および脈拍の変化

1）全例での検討

全例での収縮期血圧は観察期間168±21mmHgに対し，1剤投与期155±9mmHg，2剤併用期134±14mmHgといずれも有意に下降した。拡張期血圧は観察期間89±12mmHgに対し，1剤投与期85±11mmHgであったが，2剤併用期には77±9mmHgと有意な下降を認めた（図1）。また，全例での収縮期血圧/拡張期血圧の降圧度は，1剤投与期でそれぞれ−13±16/−5±14mmHgであったが2剤併用によりさらに−22±12/−7±10mmHg降圧し，最終降圧度は−35±17/−12±16mmHgとなった（表2）。2剤併用により血圧が140/90mmHg未満となったものは23例（61％）であった。脈

図1　全例，AⅡ受容体拮抗薬先行群および塩酸ベニジピン先行群の血圧および脈拍の変化

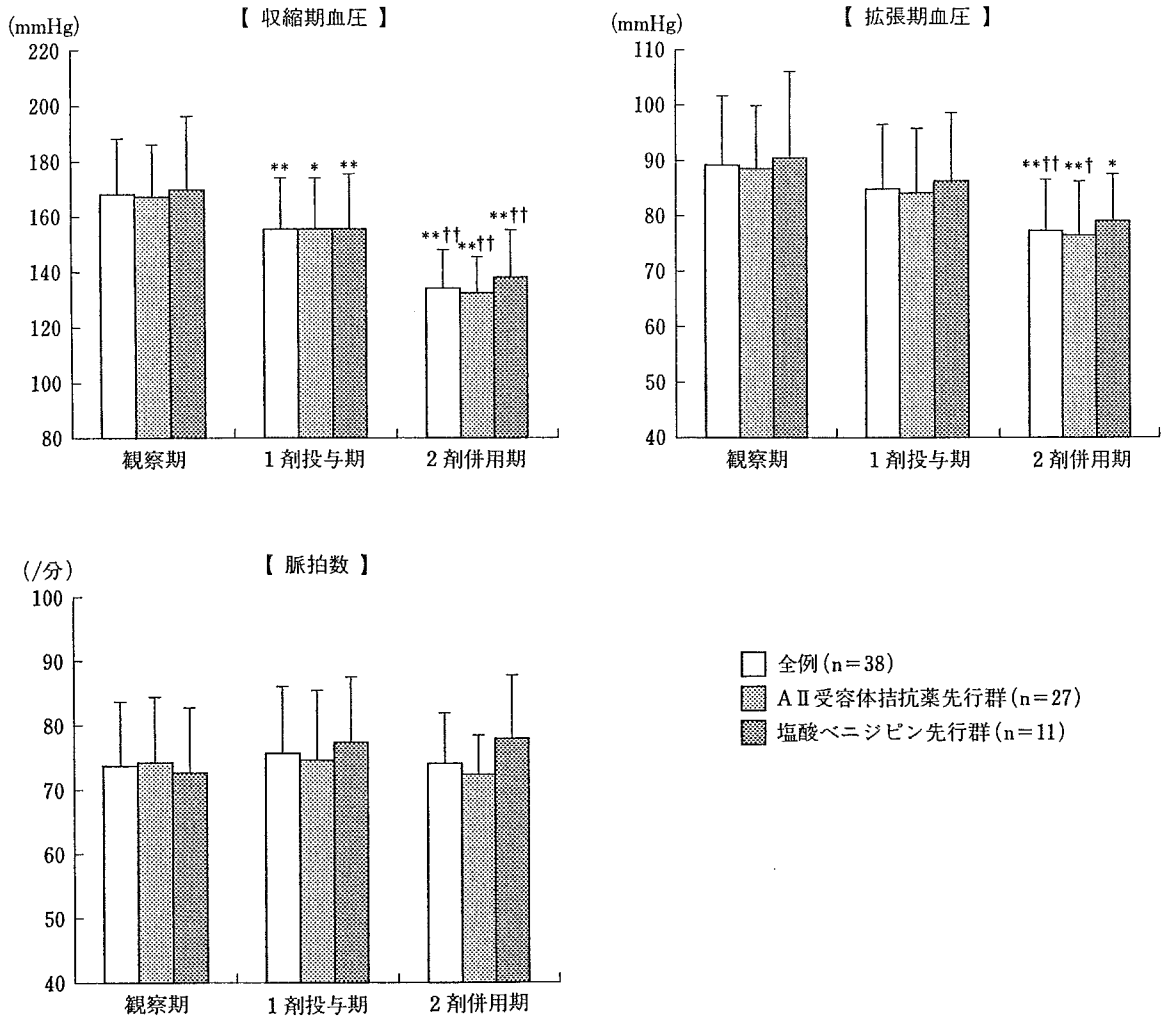

*：p<0.05，**：p<0.01；観察期に対する差　　†：p<0.05，††：p<0.01；1剤投与期に対する差

表2　降圧度と脈拍の変化

		全　例 (n=38)	AⅡ受容体拮抗薬先行群 (n=27)	塩酸ベニジピン先行群 (n=11)	
収縮期血圧 (mmHg)	1剤投与期－観察期	−13±16	−12±15	−15±20	n.s.
	2剤併用期－1剤投与期	−22±12	−23±12	−18±11	n.s.
	2剤併用期－観察期	−35±17	−35±15	−32±21	n.s.
拡張期血圧 (mmHg)	1剤投与期－観察期	− 5 ±14	− 5 ±15	− 4 ±13	n.s.
	2剤併用期－1剤投与期	− 7 ±10	− 8 ±10	− 7 ±12	n.s.
	2剤併用期－観察期	−12±16	−12±16	−12±15	n.s.
脈拍数 (/分)	1剤投与期－観察期	2 ± 8	0.1±6	5±9	n.s.
	2剤併用期－1剤投与期	− 1 ± 8	−2±7	0.5±9	n.s.
	2剤併用期－観察期	0.4±10	−2±7	6±14	n.s.

表3　AⅡ受容体拮抗薬種類別の降圧度と脈拍の変化

		ロサルタン (n=21)	カンデサルタン (n=9)	バルサルタン (n=7)	
収縮期血圧（mmHg）	2剤併用期－観察期	−34±16	−34±23	−35±13	n.s.
拡張期血圧（mmHg）	2剤併用期－観察期	−11±19	−15±14	−11±7	n.s.
脈拍数（/分）	2剤併用期－観察期	2±11	−4±10	3±4	n.s.

拍数は，観察期間，1剤投与期，2剤併用期を通じて有意な変化を認めなかった（図1）。

2）AⅡ受容体拮抗薬先行群と塩酸ベニジピン先行群間での検討

AⅡ受容体拮抗薬と塩酸ベニジピンの投与順序による降圧効果の差は認められず，脈拍も両群で有意差は認めなかった（図1，表2）。収縮期血圧/拡張期血圧の1剤投与期における降圧度は塩酸ベニジピン先行群の−15±20/−4±13mmHgに対しAⅡ受容体拮抗薬先行群では−12±15/−5±15mmHgであった。2剤併用期では塩酸ベニジピン先行群はAⅡ受容体拮抗薬追加によりさらに−18±11/−7±12mmHg，AⅡ受容体拮抗薬先行群は塩酸ベニジピン追加により−23±12/−8±10mmHgの降圧が見られ，最終平均降圧度は，それぞれ−32±21/−12±15mmHg，−35±15/−12±16mmHgに達した（表2）。2剤併用により140/90mmHg未満となったものはAⅡ受容体拮抗薬先行群で18例（67%），塩酸ベニジピン先行群で5例（45%）であった。

3）AⅡ受容体拮抗薬種類別での検討

今回テルミサルタンを投与した例は1例であったため除外し，AⅡ受容体拮抗薬と塩酸ベニジピンの投与順序を問わず，ロサルタンを投与した21例，カンデサルタンを投与した9例，バルサルタンを投与した7例で，観察期間および2剤併用後において検討した。観察期間および2剤併用後で，収縮期血圧，拡張期血圧，脈拍ともAⅡ受容体拮抗薬の種類の違いによる有意な差は認めなかった（表3）。

2. 体重，心胸郭比，血液検査データの変化

体重は全例，心胸郭比は17例，血液検査データは34例で解析可能であった。全例（表4），AⅡ受容体拮抗薬先行群，塩酸ベニジピン先行群とも，全期間を通じて体重，心胸郭比，血液生化学検査所見の有意な変化は認めなかった。

3. 自覚症状（図2）

観察期間に自覚症状を有する者は13例（34%）であり，主な自覚症状は頭痛，肩こり，動悸，気分不良，ふらつき等であった。

AⅡ受容体拮抗薬先行群では，観察期間に症状のあった11例中，AⅡ受容体拮抗薬の単独投与で7例が消失し，塩酸ベニジピンの併用投与でさらに2例が消失した。また，このAⅡ受容体拮抗薬の単独投与で症状の消失した7例中1例に塩酸ベニジピンの併用投与で症状を認めた。観察期間に症状のなかった16例中，AⅡ受容体拮抗薬の単独投与で5例に咳，ふらつき等の症状が出現したが，このうち3例は塩酸ベニジピン併用投与で消失した。また，AⅡ受容体拮抗薬の単独投与で症状のなかった11例中，塩酸ベニジピンの併用投与後1例に症状を認めた。

塩酸ベニジピン先行群では，観察期間に症状のあった2例は塩酸ベニジピンの単独投与で消失し，観察期間に症状のなかった9例は2剤併用期まで症状を認めなかった。

全体としては，試験期間中7例に新たに症状が出現した。時期別には1剤投与期に5例，および2剤併用期に2例に発現し，主な症状はふらつき，立ちくらみ，咳，倦怠感等であったが，いずれも軽度であったため投与は継続した。

表4　体重，心胸郭比，血液検査データの変化(全例)

	観　察　期	1剤投与期	2剤併用期	
体重（kg）	63±11	61±10	62±10	n.s.
心胸郭比（%）	49±4	48±6	50±6	n.s.
RBC（×10⁴/μL）	450±54	444±61	425±69	n.s.
Hg（g/dL）	14.0±1.6	13.8±1.9	13.3±2.2	n.s.
Ht（%）	41.9±4.5	40.8±5.3	39.5±6.2	n.s.
WBC（×10³/μL）	6.3±1.3	6.2±1.6	6.0±1.4	n.s.
Plt（×10⁴/μL）	22.1±5.6	22.5±5.8	21.7±5.3	n.s.
TP（g/dL）	6.9±0.5	6.8±0.6	6.8±0.8	n.s.
Alb（g/dL）	4.3±0.5	4.1±0.5	4.1±0.6	n.s.
BS（mg/dL）	117±49	135±57	120±41	n.s.
AST（IU/L）	25±12	29±17	27±20	n.s.
ALT（IU/L）	28±25	29±22	26±24	n.s.
T.bil（mg/dL）	0.7±0.3	0.6±0.3	0.7±0.3	n.s.
CPK（IU/L）	104±48	116±76	128±71	n.s.
T.cho（mg/dL）	200±35	201±29	202±32	n.s.
TG（mg/dL）	148±73	165±114	163±94	n.s.
BUN（mg/dL）	15.6±4.7	18.2±5.9	17.6±5.0	n.s.
Cre（mg/dL）	0.8±0.2	0.9±0.3	0.9±0.3	n.s.
UA（mg/dL）	5.3±1.5	5.3±1.2	5.4±1.3	n.s.
Na（mEq/L）	141±3	140±6	142±2	n.s.
K（mEq/L）	4.0±0.4	4.2±0.4	4.2±0.4	n.s.
Cl（mEq/L）	104±4	104±4	104±3	n.s.
CRP（mg/dL）	0.1±0.2	0.2±0.3	0.2±0.1	n.s.

RBC＝赤血球数，Hg＝ヘモグロビン，Ht＝ヘマトクリット，WBC＝白血球数，Plt＝血小板数，TP＝総蛋白，Alb＝アルブミン，BS＝血糖，T.bil＝総ビリルビン，T.cho＝総コレステロール，TG＝中性脂肪，Cre＝クレアチニン，UA＝尿酸

4. 安全性

血液検査所見，体重，心胸郭比とも全期間を通じて有意差は認めなかった（表4）。AII受容体拮抗薬を2剤目として追加投与後，血清クレアチニンが1.0から1.3に上昇した例を1例認めたが，軽度であったため主治医の判断で投薬を継続した。

Ⅳ 考　　察

今回我々は本態性高血圧患者において，塩酸ベニジピンとAII受容体拮抗薬の併用療法の有用性を検討した。両者の併用により良好な降圧効果が得られた。また，降圧による反射性頻脈や検査データの重篤な悪化，投薬を中止するよ